

Ultrasonic vibration-assisted microgrinding of glassy carbon

Patrick Beiring¹ and Jiwang Yan² 

Proc IMechE Part C:
J Mechanical Engineering Science
 2019, Vol. 233(12) 4165–4175
 © IMechE 2019
 Article reuse guidelines:
sagepub.com/journals-permissions
 DOI: 10.1177/0954406218823240
journals.sagepub.com/home/pic



Abstract

Glassy carbon is an amorphous material which, due to its unique material properties, has recently been introduced to micro/nanoimprinting as mold substrates. However, since glassy carbon is a hard, brittle, and highly elastic material, the precision machining of micro/nanostructures on it remains a challenging task. In this research, ultrasonic vibration-assisted microgrinding was proposed for ductile machining of glassy carbon. To find suitable conditions, the effects of ultrasonic vibration assistance and tool inclination were investigated. The results showed that by utilizing ultrasonic vibration assistance and tool inclination, a ductile response was achieved with improved surface roughness. In addition, the periodical waviness of the groove edge due to material elastic recovery was successfully prevented. This study provided an insight into the kinematics in ultrasonic vibration-assisted grinding of a highly elastic, hard, and brittle material.

Keywords

Glassy carbon, ultrasonic vibration, microstructure, microgrinding, hard brittle material, surface integrity

Date received: 15 April 2018; accepted: 14 December 2018

Introduction

Glassy carbon (GC) is an amorphous material, which has been used as molds for glass molding press. This is due to its high-temperature resistance, chemical stability, and unique mechanical properties. Furthermore, it has recently been used as a mold substrate for imprinting of micro/nanostructures on glass and polymers.^{1,2} Previously, laser machining has been introduced to fabricate such molds. However, laser machining generally results in a high surface roughness within the machined groove, and additionally, it is difficult to control the cross-sectional groove geometry. Another approach is to use focused ion beam (FIB) machining to machine GC in the nanometer scale. However, FIB is an extremely time-consuming method due to the fact that it has extremely low material removal rates,^{3,4} and has difficulties to machine submillimeter-size grooves on a large-area surface. Thus, it is important to overcome the problems of these high-energy beam machining methods and realize high-precision machining of submillimeter-size microstructures on GC with high surface integrity in a short machining time. Microgrinding, as a mechanical machining method, might offer a suitable solution to these problems.

Microgrinding provides a feasible solution to high-efficiency machining of microstructures on a large-area surface with surface roughness in the nanometer level. The ductile regime grinding has been previously

investigated for many other hard brittle materials, such as silicon, fused silica, and BK7 glass, which provided a suitable answer to the manufacturing requirements of semiconductor substrates and optical components.^{5,6} However, most of the research on ductile grinding has been carried out for flat or curved continuous surfaces by using big grinding wheels (diameter of 100 mm level), whereas the literature on slot grinding of grooves by using small-diameter (~ submillimeter) pencil tools are very limited. Especially, since GC is a hard, brittle, and highly elastic material, the precision machining of microgrooves on GC still remains a challenge.

In microgrinding of grooves on hard brittle materials, the reduction of grinding force is a critical task. In recent years, the use of ultrasonic vibration for assisting end milling, grinding, and other mechanical manufacturing methods has been attempted to produce better surface integrity, lower cutting forces,

¹Graduate School of Science and Technology, Keio University, Yokohama, Japan

²Department of Mechanical Engineering, Faculty of Science and Technology, Keio University, Yokohama, Japan

Corresponding author:

Jiwang Yan, Department of Mechanical Engineering, Faculty of Science and Technology, Keio University, Hiyoshi 3-14-1, Kohoku-ku, Yokohama, Kanagawa 223-8522, Japan.
 Email: yan@mech.keio.ac.jp

and lower tool wear.^{7–12} In addition to the aforementioned positive effects of ultrasonic vibration-assisted machining, the ultrasonic vibration assistance has also shown to facilitate the transition from brittle to ductile material removal mode and reduce the crack generation of brittle materials.^{13–16}

Due to the challenges of microgroove machining in GC, it is the purpose of this study to propose an ultrasonic vibration-assisted grinding (UVAG) process with tool inclination in order to take advantage of the kinematic improvements of the ultrasonic vibration, and therefore solve the aforementioned difficulties to improve the surface quality and groove edge integrity, as well as to reduce the grinding force. Especially, it is expected that the ultrasonic vibration can facilitate to solve the problems caused by the high elasticity of the workpiece material through the improved kinematics.

Kinematics of vibration-assisted microslot grinding

The vibration-assisted microslot grinding process has two different characteristics when compared with conventional surface grinding. On one hand, the side-walls are removed in up-grinding or down-grinding modes, and on the other hand, the groove bottom follows a cyclic indentation and scratching process due to the ultrasonic vibration. Furthermore, the use of ultrasonic vibration also changes the kinematic motions of the grains in a way that the ultrasonic vibration is superimposed to the conventional rotation of the grinding wheel.

Side-surface formation

A single abrasive–workpiece interaction model for surface grinding and a schematic model for microslot grinding process are depicted in Figure 1(a) and (b), respectively. In Figure 1(a), the maximum chip thickness h_{max} is the distance from C to A. In the grinding process of side-walls, up-grinding and down-grinding take place during the revolution of the tool, as shown in Figure 1(b). For the up-grinding part, the undeformed chip thickness starts at zero when the grain engages with the side-walls of the workpiece and reaches its maximum in the middle of the groove. In contrast, the down-grinding starts with the maximum and reaches zero at the side-wall of the groove. In slot grinding, the maximum chip thickness h_{max} is defined by the circumferential speed of tool v_s , the workpiece velocity v_w , and the space L between two consecutive grains, as expressed by the following

$$h_{max} = L \frac{v_w}{v_s} \quad (1)$$

The value of h_{max} is equal for both up-grinding and down-grinding. If the value of the undeformed chip thickness h reaches the critical undeformed chip

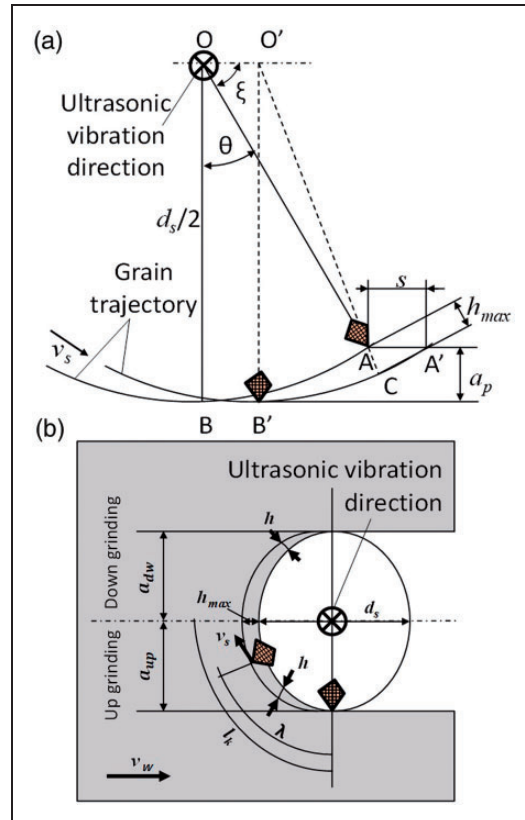


Figure 1. Models for interaction between a single abrasive grain and workpiece in (a) surface grinding and (b) microslot grinding.

thickness d_c for the ductile–brittle transition, then brittle fracture will occur during the grinding process. Considering that the brittle fracture is sufficiently far away from the side-walls, it is possible that the fractures are removed during the subsequent grinding pass, resulting in a ductile-machined surface. When the undeformed chip thickness is below the critical value, however, plastic deformation dominates material removal and complete ductile regime grinding is realized.

Groove bottom formation

Unlike the side-wall grinding process, the abrasives at the end face of the tool are not always in contact with the workpiece. As depicted in Figure 2, the grains periodically indent into the workpiece with a total penetration depth δ . In case of brittle mode machining, median and lateral cracks form during each workpiece–grain contact cycle,¹⁷ among which lateral cracks are responsible for the material removal. However, when ductile material removal mode is achieved, only the plastic deformation zone dominates the material removal.

Grain trajectories

In general, the grain trajectories can be divided into two different situations. Firstly, considering the

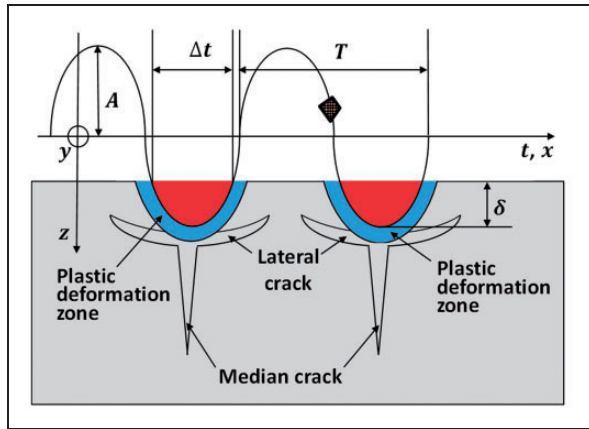


Figure 2. Kinematic abrasive–workpiece interaction model at the end face of a tool.¹⁶

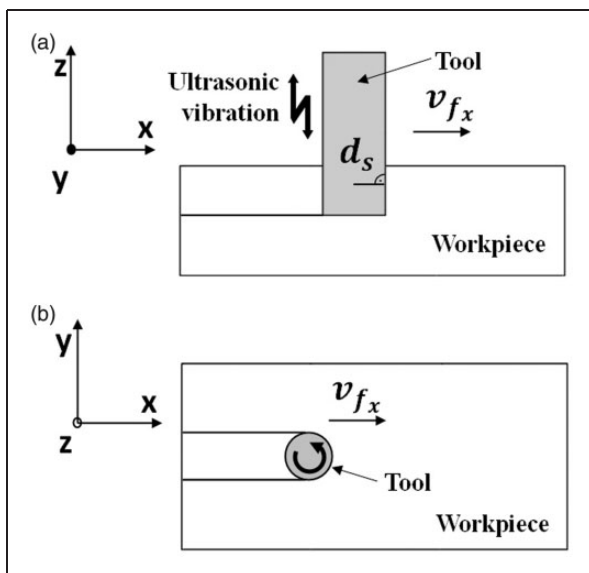


Figure 3. Schematic illustration of UVAG without tool inclination. (a) Front view and (b) Top view.

coordinate system $x-y-z$ given in Figure 3 and the origin of the coordinate system lying on the rotational axis of the tool, the trajectories can be expressed as equation (2), where d_s is the grinding tool diameter, ω_s and ω_v the angular frequency of the spindle and the vibration respectively, v_{fx} the feed rate in x -direction, and A the amplitude of the vibration

$$\begin{cases} x = \frac{d_s \sin(\omega_s t)}{2} + v_{fx} t \\ y = \frac{d_s \sin(\omega_s t)}{2} \\ z = A \sin(\omega_v t) \end{cases} \quad (2)$$

For the microslot grinding of the side-faces, the following equations for the grain trajectory length l_k

can be derived according to Figure 1

$$l_k = \int_0^\theta dl_k + \frac{s}{2} \quad (3)$$

$$l_k = \left(1 \pm \frac{v_w}{v_s}\right) \frac{d_s \theta}{2} + \frac{\theta^3}{6\left(1 \pm \frac{v_w}{v_s}\right)} + \frac{s}{2} \quad (4)$$

Furthermore, an important factor to denote the total grain trajectory length is the time t_c during which the grain is in contact with the workpiece. Li et al.¹⁸ suggested an approach to express t_c with the cutting depth a_p

$$a_p = \frac{d_s}{2} - \frac{d_s}{2} \cos\left(\frac{2\pi n_s}{60} t_c\right) \quad (5)$$

$$\cos\left(\frac{2\pi n_s}{60} t_c\right) = 0 \quad (6)$$

$$t_c = \frac{60}{4n_s} \quad (7)$$

From equation (5), equation (6) is induced for the reason that the cutting depths a_p equals to half the tool diameter for microslot grinding. Furthermore, the cosine takes the value of 1 in this case, due to the fact that the maximum angle for both up- and down-grinding is 90° . Finally, considering equations (3) to (7), the following equation for the total grain trajectory length l can be derived which has an additional term to the conventional surface grinding term given by l_k

$$l = \sqrt{l_k^2 + \left(\frac{t_c}{T} 4A\right)} \quad (8)$$

Tool inclination

It is well known that for ball end milling, an inclined tool showed better surface integrity than that without tool inclination. When milling a brittle material, the brittle-to-ductile transition mechanism was also affected by tool inclination. The tool inclination compensated the disadvantages of edge roughness, and an inclination angle of 45° was found to be most suitable for ductile regime machining.^{19,20} Similar results have been reported for the grinding process when machining microstructured surfaces on brittle materials.¹² A 45° inclination angle was used successfully to machine several different surface structures in ductile mode on brittle materials. The improved surface quality was due to an increase in the trace length of abrasive grains and an overlap of the traces of the grains, which resulted in reduced grinding marks on the machined surface. These previous researches

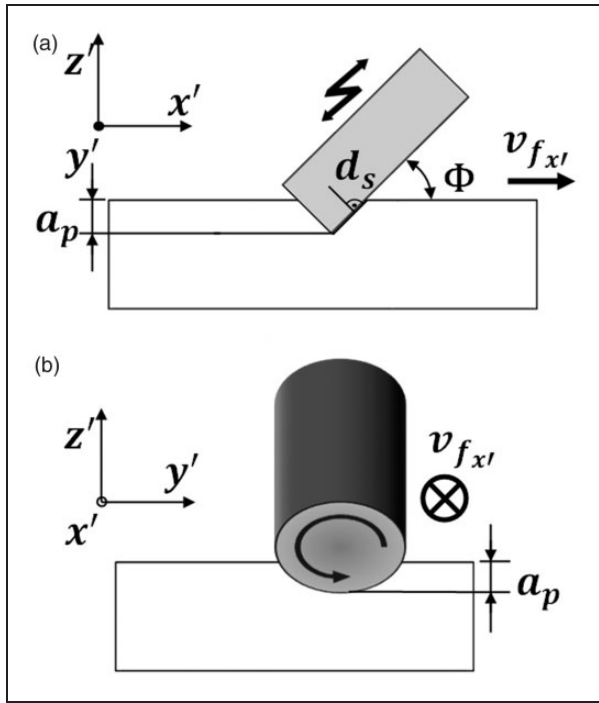


Figure 4. Schematic illustration of UVAG with tool inclination. (a) Front view and (b) Side view.

showed promising results for improving the surface integrity, shape accuracy and the edge quality for groove machining of brittle materials for both milling and grinding. For this reason, tool inclination was attempted in this study.

Considering the coordinate system $x'y'z'$ given in Figure 4 and the origin of the coordinate system lying on the rotational axis of the tool, similar equations for the combined motions of the conventional grinding, the ultrasonic vibration with tool inclination can be expressed as equation (9), where d_s is the grinding tool diameter, ω_s and ω_v the angular frequencies of the spindle and the vibration respectively, A the amplitude of the vibration, and Φ the inclination angle of the tool:

$$\left\{ \begin{array}{l} x' = \frac{d_s \sin(\omega_s t)}{2} \cos(\Phi) + v_{fx'} t + A \sin(\omega_v t) \cos(\Phi) \\ y' = \frac{d_s \sin(\omega_s t)}{2} \\ z' = A \sin(\omega_v t) \sin(\Phi) + \frac{d_s \cos(\omega_s t)}{2} \sin(\Phi) \end{array} \right. \quad (9)$$

From the aforementioned equations, it is apparent that the grain trajectories with tool inclination ultrasonic vibration generally have a longer interaction path with the workpiece compared to the conventional grinding. The applicability of the equations was also confirmed by Li et al.¹⁸ who investigated the influence of the ultrasonic vibration on the grain

Table 1. Grinding conditions for UVAG with tool inclination.

Item	Value
Tool diameter	1 mm
Abrasive grain size	25 µm
Rotation rate	5000, 6000, 7000 r/min
Feed rate	1, 2, 3, 20, 30 µm/s
Grinding depth	70 µm
Inclination angle	0°, 45°
Vibration amplitude	1.44–1.72 µm
Environment	Dry, soluble oil

trajectory length, grinding force and surface finish. When the material removal volume for both processes is the same, the following advantages can be achieved by UVAG: smaller grinding chips, smaller forces, and better surface integrity.^{18,20–22}

Experimental details

Experiments of UVAG with tool inclination were performed to analyze the material removal behavior in the grooving process. A four-axis numerical controlled ultraprecision machine tool was used for grinding. The experimental conditions are shown in Table 1. The groove depth was set to 70 µm for all experiments. The SEM photographs of an electroplated grinding tool and a close view of its surface are shown in Figure 5(a) and (b). The tool has a diameter of 1 mm. Diamond abrasive grains with an average grain size of 25 µm were electroplated on the tool surface. The specimens were GC prefabricated with dimensions of 50 mm in length, 20 mm in width, and 5 mm in thickness. A photograph of the specimen is presented in Figure 6. GC sample is a highly elastic material with a Young's modulus ranging from 21 to 22.5 GPa. For comparison, tungsten carbide has a minimum Young's modulus of 600 GPa.¹

The ultrasonic vibration unit used in this study consisted of an ultrasonic generator, a piezoelectric device and a horn for amplification of the vibration. These were attached to the machine spindle as illustrated in Figure 7. By applying an AC voltage to the piezoelectric element a vibration is generated, which is amplified by the horn. Ultrasonic vibration occurs along the tool axis with a frequency ranging from 24 kHz to 27 kHz and an amplitude from 1.44 µm to 1.72 µm. Figure 8 shows a photograph of the experimental setup, and Figure 9 shows the situation of grinding experiments with a tool inclination angle of 45°.

A scanning electron microscope (SEM) and an optical microscope were used to observe the machined surfaces to identify whether ductile regime grinding was achieved. A laser probe microscope and a white-light interferometer were used to measure the

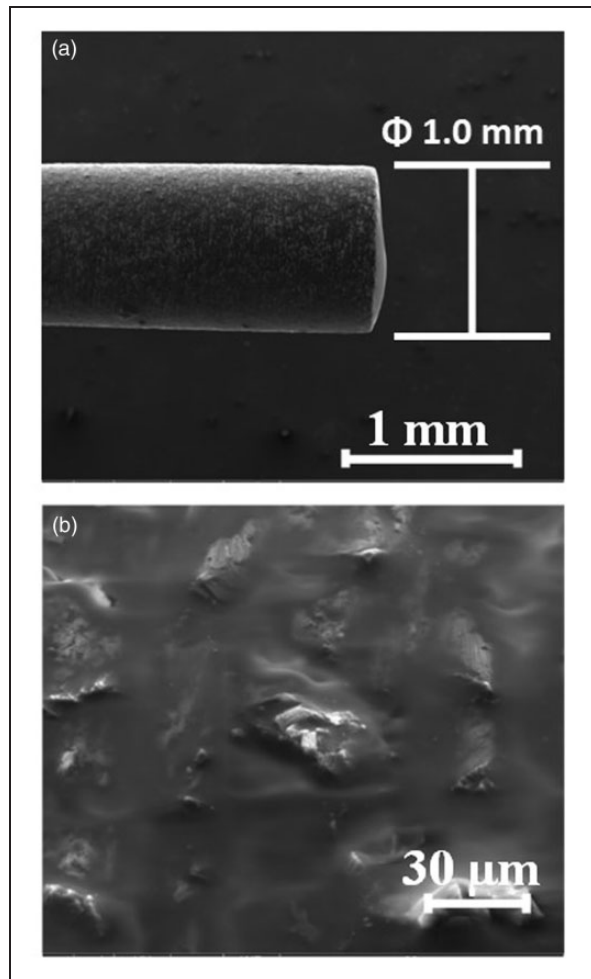


Figure 5. SEM photographs of (a) an electroplated tool and (b) the tool surface.



Figure 6. Photograph of a GC workpiece.

two-dimensional and three-dimensional groove profiles and surface roughness, respectively, under different feed rates, inclination angle, spindle speeds, and vibration amplitudes for the ultrasonic vibration assistance. In addition, a piezoelectric dynamometer (Kistler 9119AA2) was installed on the machine table to measure the grinding forces.

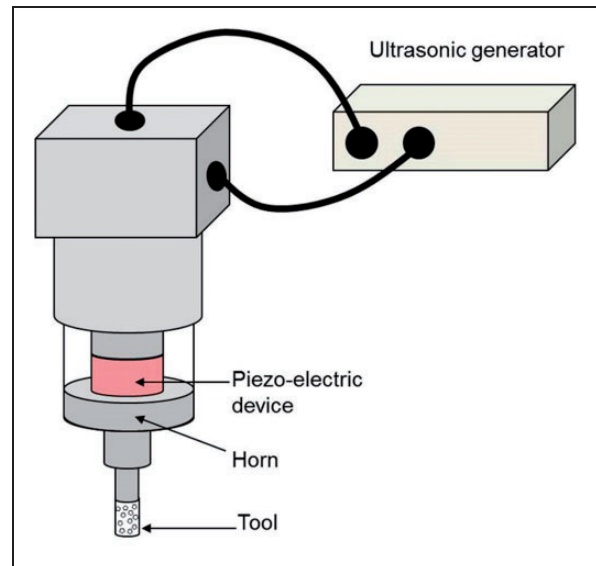


Figure 7. Schematic diagram of the ultrasonic vibration unit.

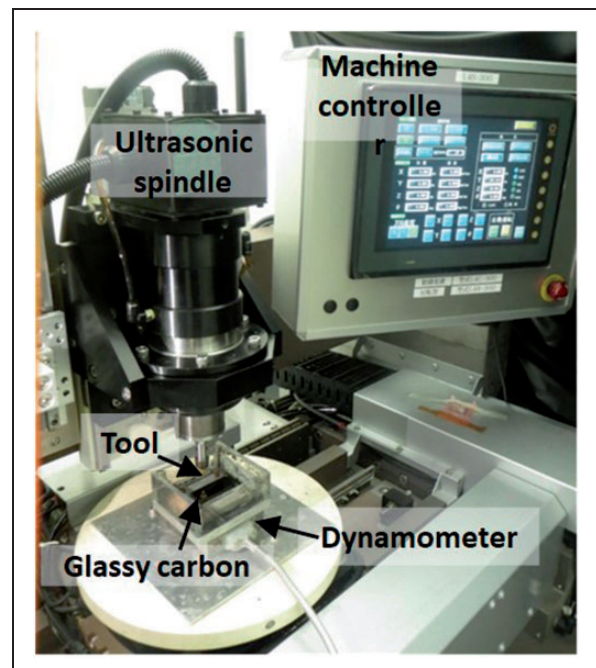


Figure 8. Photograph of the experimental setup for microgrinding.

Results and discussion

Surface integrity for UVAG without tool inclination

Figure 10 shows the influence of ultrasonic vibration amplitude on surface roughness R_a at a constant tool feed rate of $1\text{ }\mu\text{m/s}$. The surface roughness measurements were done at the bottom of the rectangular groove and the average surface roughness from five measurements was evaluated. It can be seen that when the amplitude was $1.60\text{ }\mu\text{m}$, the surface roughness was

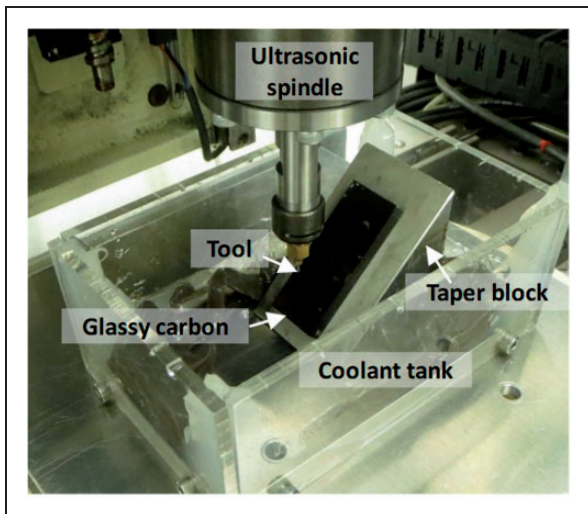


Figure 9. Photograph of the setup for microgrinding with tool inclination.

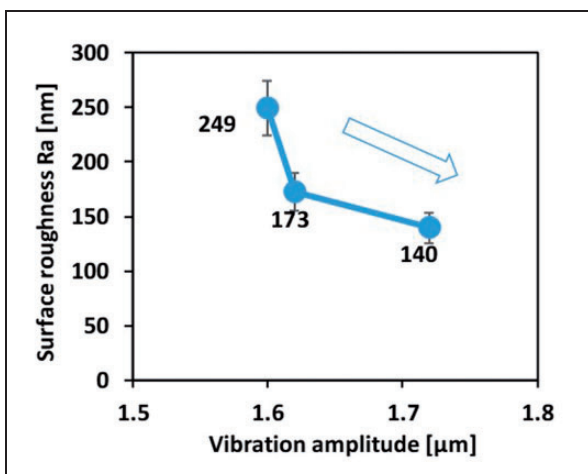


Figure 10. Influence of vibration amplitude on surface roughness.

249 nm Ra, whereas a higher vibration amplitude (1.72 μm) resulted in a reduction of surface roughness to 140 nm Ra.

Figure 11(a) and (b) shows the SEM images of typical surface areas obtained at vibration amplitudes of 1.60 μm and 1.72 μm . The surface machined at a vibration amplitude of 1.60 μm is covered by both microfractures and protrusions due to material adhesion. In contrast, the surface machined at an amplitude of 1.72 μm is generally smooth without material adhesion, although a few microfractures are seen. This can be explained with the kinematics of the ultrasonic vibration motion on the end face of the grinding tool. An increase in vibration amplitude improved debris removal from the gap between tool and workpiece, thus prevented material adhesion on the machined surface. Further surface measurement using a white light interferometer showed that the

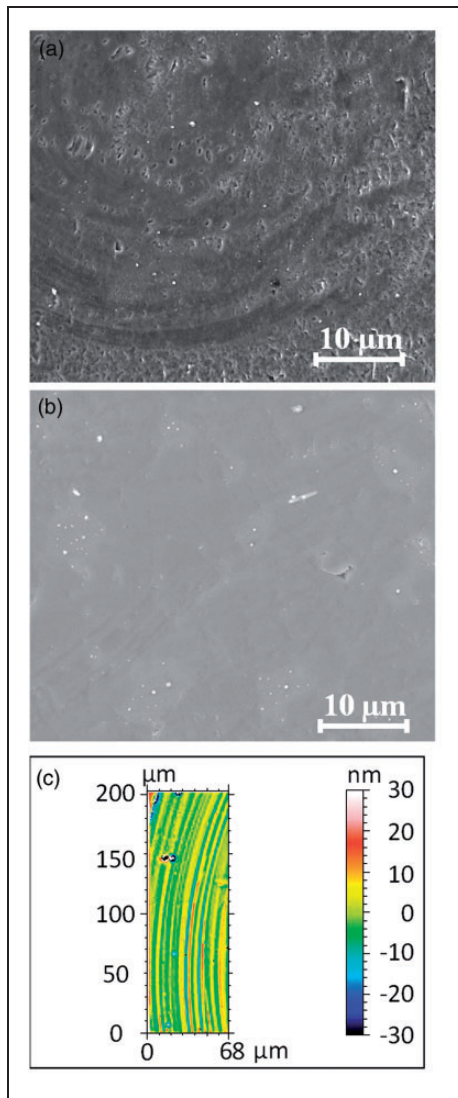


Figure 11. SEM photographs of machined surfaces on the groove bottom at different vibration amplitudes: (a) 1.60 μm , (b) 1.72 μm . (c) is the surface topography of a small surface region in (b) measured by white light interferometer.

local surface roughness of some smooth surface regions reached ~ 6 nm Sa (see Figure 11(c)). This indicates that complete ductile mode grinding is possible under optimized conditions. However, grinding tools available in this experiment were electroplated with coarse abrasive grains, thus some surface regions involved scratches and microfractures. The scratches and microfractures appeared intensively on certain grinding traces, which might be caused by some highly protruding abrasive grains.

Figure 12 shows the influence of tool feed rate on surface roughness at a constant ultrasonic vibration amplitude of 1.72 μm . The surface roughness Ra for microslot grinding of GC showed an increasing trend for higher feed rates. At a feed rate of 1 $\mu\text{m}/\text{s}$, a surface roughness of 140 nm was obtained. As the feed rate increased to 2 $\mu\text{m}/\text{s}$ and 3 $\mu\text{m}/\text{s}$, the surface roughness increased to 160 nm and 194 nm, respectively. As the feed rate increased, the undeformed chip

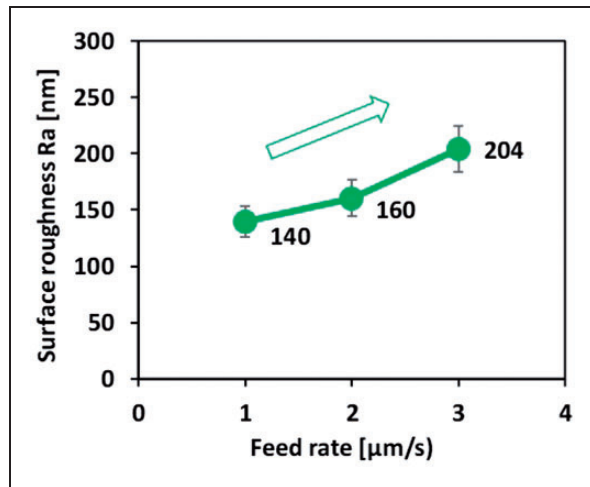


Figure 12. Influence of tool feed rate on surface roughness.

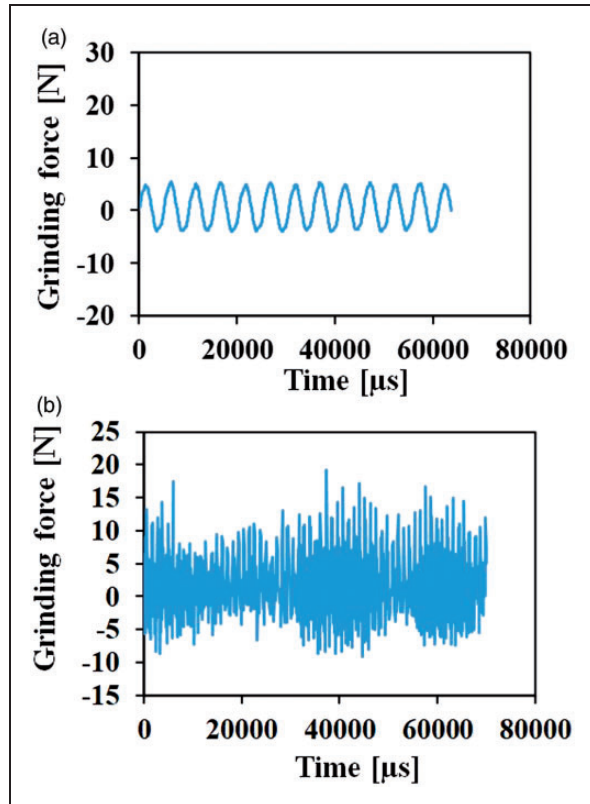


Figure 13. Grinding force comparison between (a) ductile mode machining and (b) brittle mode machining.

thickness for each grain on the grinding wheel increased as well, therefore the possibility of brittle fracture generation was raised.

Grinding forces for ductile and brittle regimes showed significant differences in their patterns. For the ductile grinding mode, the force signal showed a very smooth waveform as shown in Figure 13(a). On the other hand, the force measurements from a groove machined in a brittle mode showed a high fluctuation,

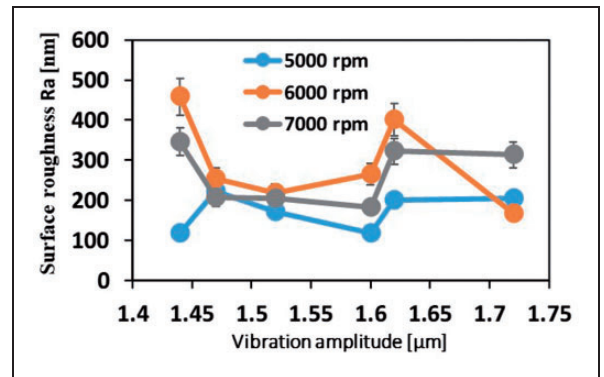


Figure 14. Surface roughness variation for different spindle rotation rates with tool inclination.

which indicates a more instable process, as seen in Figure 13(b). This is due to the different material removal mechanisms. Ductile removal of material is performed by plastic deformation, which results in a very smooth force signal without fluctuation. In brittle mode material removal, due to the randomly forming cracks, the grinding force was fluctuated significantly.²³

Surface integrity for UVAG with tool inclination

Figure 14 shows the surface roughness results obtained by using tool inclination at an angle of 45° at different spindle speeds from 5000 r/min to 7000 r/min and ultrasonic vibration amplitudes. Measurements were performed along the entire curved groove including the entry and the exit sides. The values obtained in every five measurements were averaged and then plotted in Figure 14. At a spindle speed of 5000 r/min and a vibration amplitude of 1.44 μm, a surface roughness of 118 nm Ra was obtained. The average surface roughness was below 200 nm Ra. Among the three spindle rotation rates used, the lowest surface roughness was obtained at 5000 r/min and the highest at 6000 r/min for all vibration amplitudes except 1.44 μm and 1.72 μm. This indicates that when using an inclined tool, there might be interaction between spindle rotation rate and vibration amplitude. It is necessary to optimize the combination of the two parameters for surface roughness improvement.

It is also noted that in Figure 14, the effect of vibration amplitude on surface roughness is complicated, and different from the trend shown in Figure 10. As seen from equation (9) and Figure 4, the vibration amplitude can be divided into two components: one is perpendicular to and the other is tangential to the workpiece surface. The effectiveness of the tangential vibration assistance lies in the increase of grain trajectory length. When the amplitude of the vibration increases, the trajectory length for each grain increases as well. As a result, the grinding force and surface roughness decrease.¹⁸ On the other hand, the

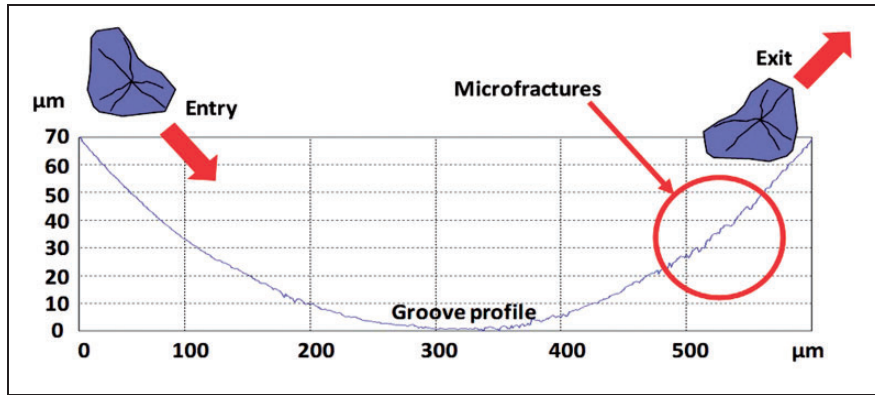


Figure 15. A cross-sectional groove profile obtained by grinding with tool inclination, showing different topological features at the entry and exit sides.

effect of the perpendicular component of vibration amplitude on surface roughness in inclination grinding is different from that in noninclination grinding. In inclination grinding, the debris adhesion on machined surface is insignificant. As a result, an increase in the perpendicular component of vibration amplitude will increase surface roughness due to the indentation effect shown in Figure 2.

Further investigations of the groove profile have shown that the surface topology of the entry and the exit of the grooves were different, as shown in Figure 15. More microfractures were observed on the exit side than the entry side. Five measurements of surface roughness were performed at the entry and at the exit of a groove, averaged and then compared in Figure 16. For all spindle rotation rates and vibration amplitudes, the surface roughness at the exit side is higher than that at the entry side. For the spindle rotation rate of 5000 rpm, a minimum surface roughness of 86 nm Ra was obtained at the entry side of the groove. In contrast, the corresponding value at the exit side is 159 nm Ra. At the entry side of the groove, undeformed chip thickness increases as the tool advances, thus the material is squeezed into the bulk and a high compressive stress is generated. The compressive stress is beneficial for promoting the ductile response of material. At the exit side, however, undeformed chip thickness decreases as the tool advances and the squeezing effect is weakened, leading to a lower compressive stress in the material, as shown in Figure 17. Therefore, the surface roughness of exit side is higher than that of the entry side.

Effect of tool vibration on groove edge formation

In conventional grinding of GC, the high elasticity of the workpiece material becomes a problem. As shown in Figure 18(a), the edge of the machined groove is not straight, but becomes wavy. The diameter of the fitting curve of the edge wave (912 μm) is similar to the tool diameter (1 mm). This phenomenon is especially significant when a small tool feed rate is used.

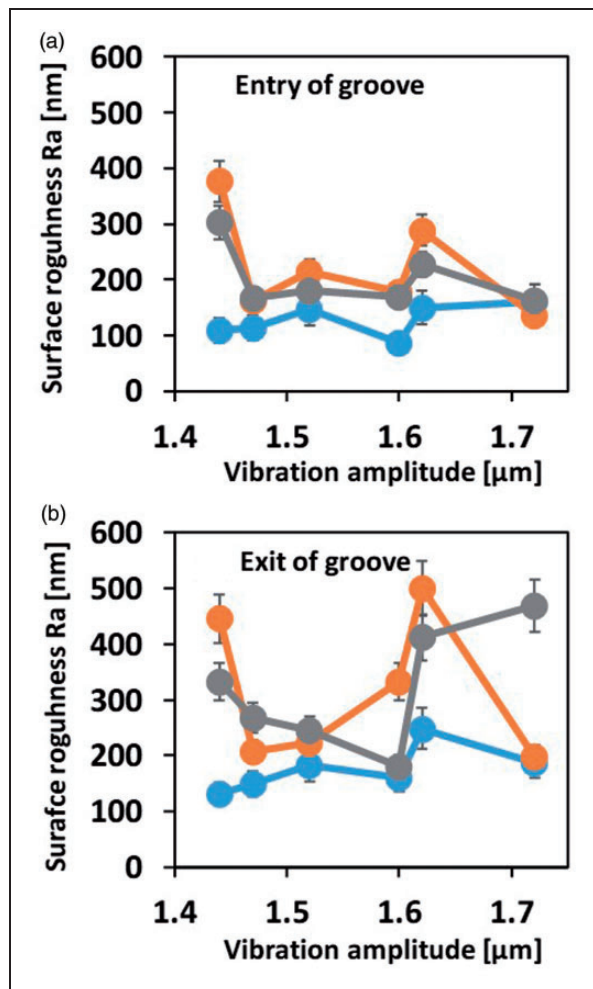


Figure 16. Surface roughness measurements for the entry and the exit sides of the grooves. (a) Entry of groove (b) Exit of groove.

However, when applying ultrasonic vibration to the tool, the edge waviness problem was completely solved. The groove edge becomes very straight as shown in Figure 18(b).

The edge waviness phenomenon was caused by the high elasticity of the GC material. At a low tool feed

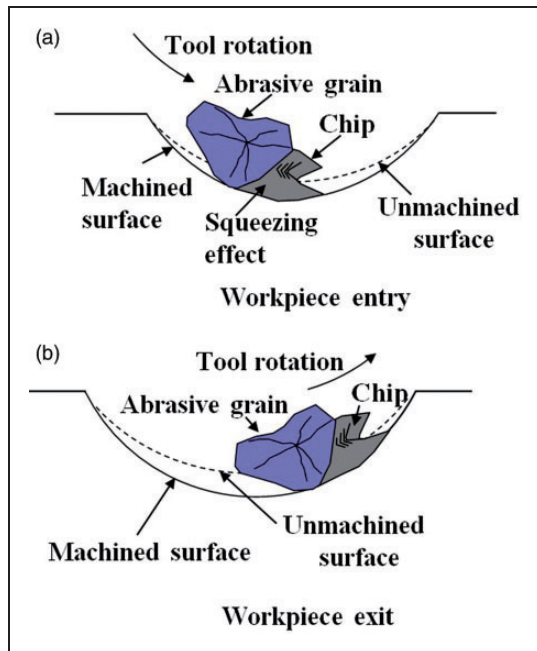


Figure 17. Kinematics of the grinding behavior at the (a) entry side and (b) exit side of a single groove.

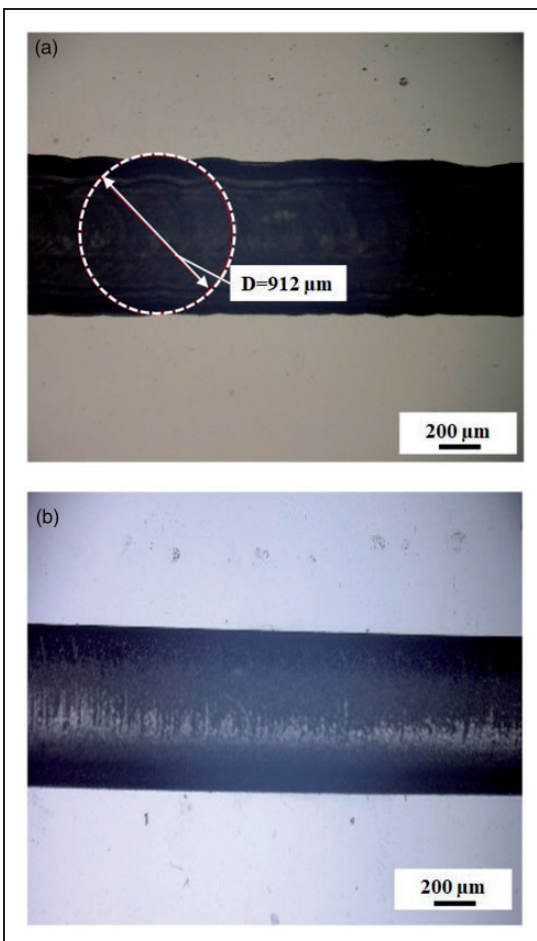


Figure 18. Photographs of grooves showing (a) wavy edges machined by microgrinding without ultrasonic vibration and (b) smooth edges machined by UVAG.

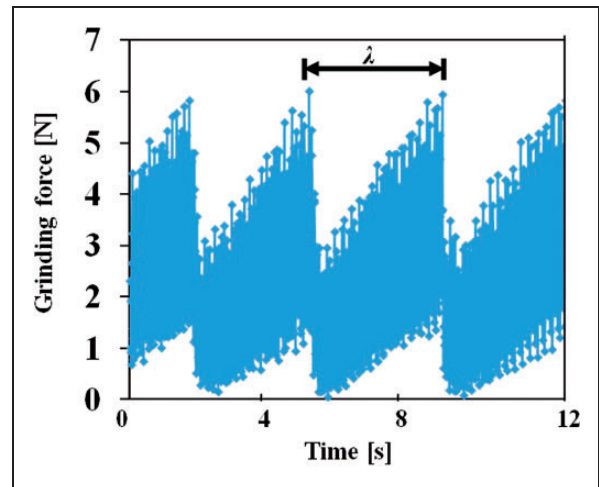


Figure 19. Periodic force pattern for microgrinding without ultrasonic vibration (tool feed rate 30 $\mu\text{m}/\text{s}$).

rate, the undeformed chip thickness per tool revolution is very small compared with the radius of the abrasive grains. As a result, the material cannot be removed, and slip against the tool. As the tool is further fed and the undeformed chip thickness is accumulated due to the material elastic deformation. When the elastic deformation is accumulated to a certain extent, material removal begins suddenly due to elastic recovery, leaving curved marks on the groove edge. The wavy edge formation corresponds to a periodic force pattern as seen in Figure 19, where the force rises to a high value and is then released to nearly zero. The approximate cycle time λ for each period is 4 s, which is the same as the time periodicity of the edge waviness. Kim et al.²⁴ discussed the periodic force pattern for micromilling and attributed this effect to the reason that in micromachining, the tool does not remove material with each rotation, it rather deforms the workpiece material until the minimum chip thickness is reached. Similar problems occur to the grinding process.

However, in UVAG of GC, the force pattern is different. As seen in Figure 13, the force follows a stable sine wave form without accumulation-release phenomenon. Due to the superposition of ultrasonic vibration, the machining of the highly elastic GC becomes stable with generating straight groove edges even at a low tool feed rate.

Conclusions

Machining characteristics in microslot grinding of GC with ultrasonic vibration-assistance and tool inclination were experimentally investigated. The results indicated that without tool inclination, as the vibration amplitude increases the surface gets smoother due to the prevention of debris adhesion to the machined surface. An increase in the feed rate increases surface roughness. Tool inclination improved surface roughness to $\sim 200 \text{ nm Ra}$. Differences in entry and exit

sides of the groove have been found. The entry side of the groove showed a higher surface integrity than the exit side. Furthermore, the groove edge waviness problem caused by the high elasticity of GC was successfully solved by the ultrasonic vibration-assisted grinding. This study demonstrated the possibility of machining microstructures on glassy carbon in a ductile mode by ultrasonic vibration-assisted microgrinding. As future work, surface roughness is to be further improved by using finer abrasive grains for the electroplated grinding tools, and the optimization of the interaction between spindle rotation rate and vibration amplitude is necessary.

Declaration of Conflicting Interests

The author(s) declared no potential conflicts of interest with respect to the research, authorship, and/or publication of this article.

Funding

The author(s) received no financial support for the research, authorship, and/or publication of this article.

ORCID iD

Jiwang Yan  <http://orcid.org/0000-0002-5155-3604>

References

- Garion C. Mechanical properties for reliability analysis of structures in glassy carbon. *World J Mech* 2014; 4: 79–89.
- Parker SF, Imberti S, Callear SK, et al. Structural and spectroscopic studies of a commercial glassy carbon. *Chem Phys* 2013; 427: 44–48.
- Tseng S-F, Chen M-F, Hsiao W-T, et al. Laser micro-milling of convex microfluidic channels onto glassy carbon for glass molding dies. *Opt Lasers Eng* 2014; 57: 58–63.
- Youn SW, Takahashi M, Goto H, et al. Microstructuring of glassy carbon mold for glass embossing – comparison of focused ion beam, nano/femtosecond-pulsed laser and mechanical machining. *Microelectron Eng* 2006; 83: 2482–2492.
- Wang W, Yao P, Wang J, et al. Crack-free ductile mode grinding of fused silica under uncontrollable dry grinding conditions. *Int J Mach Tools Manuf* 2016; 109: 126–136.
- Gu W, Yao Z and Li H. Investigations of grinding modes in horizontal surface grinding of optical glass BK7. *J Mater Process Technol* 2011; 211: 1629–1636.
- Brinksmeier E, Mutlugün Y, Klocke F, et al. Ultra-precision grinding. *CIRP Ann* 2010; 59: 652–671.
- Bhaduri D, et al., Ultrasonic assisted creep feed grinding of Inconel 718. In: *CIRP conference on electro physical and chemical machining*, Leuven, Belgium, 9–12 April 2013, pp.615–620.
- Chen JB, Fang QH, Wang CC, et al. Theoretical study on brittle-ductile transition behavior in elliptical ultrasonic vibration assisted grinding of hard and brittle materials. *Precis Eng* 2016; 46: 104–117.
- Gong H, Fang FZ and Hu XT. Kinematic view of tool life in rotary ultrasonic side milling of hard and brittle materials. *Int J Mach Tools Manuf* 2010; 50: 303–307.
- Brehl E and Dow TA. Review of vibration-assisted machining. *Precis Eng* 2008; 32: 153–172.
- Guo B and Zhao Q. Ultrasonic vibration assisted grinding of hard and brittle linear micro-structured surfaces. *Precis Eng* 2017; 48: 98–106.
- Zhou M, Wang XJ, Ngoi BKA, et al. Brittle-ductile transition in the diamond cutting of glasses with the aid of ultrasonic vibration. *J Mater Process Technol* 2002; 121: 243–251.
- Wang J, Zha H, Feng P, et al. On the mechanism of edge chipping reduction in rotary ultrasonic drilling: a novel experimental method. *Precis Eng* 2016; 44: 231–235.
- Uhlmann E, Protz F, Stawiszynski B, et al. Ultrasonic assisted milling of reinforced plastic. In: *1st CIRP conference on composite materials parts manufacturing*, Karlsruhe, Germany, 3–9 June 2017, pp.164–168.
- Wang J, Zhang J, Feng P, et al. Damage formation and suppression in rotary ultrasonic machining of hard and brittle materials: a critical review. *Ceram Int* 2018; 44: 1227–1239.
- Marshall DB, Lawn BR and Ewans AG. Elastic/plastic indentation damage in ceramics: the lateral crack system. *J Am Ceram Soc* 1982; 65: 561–566.
- Li C, Zhang F, Meng B, et al. Material removal mechanism and grinding force modelling of ultrasonic vibration assisted grinding of SiC ceramics. *Ceram Int* 2017; 43: 2981–2993.
- Foy K, Wei Z, Matsumura T, et al. Effect of tilt angle on cutting regime transition in glass micromilling. *Int J Mach Tools Manuf* 2009; 49: 315–324.
- Matsumura T and Ono T. Cutting process of glass with inclined ball end mill. *J Mater Process Technol* 2008; 200: 356–363.
- Guo B, Zhao Q-L and Jackson MJ. Ultrasonic vibration-assisted grinding of micro-structured surfaces on silicon carbide ceramics materials. *Proc IMechE, Part B: J Engineering Manufacture* 2011; 226: 553–559.
- Cheng J, Wang C, Wen X, et al. Modelling and experimental study on micro-fracture behavior and restraining technology in micro-grinding of glass. *Int J Mach Tools Manuf* 2014; 85: 36–48.
- Arif M, Rahman M and San WY. Ultraprecision ductile mode machining of glassy by micromilling process. *J Manuf Process* 2011; 13: 50–59.
- Kim CJ, Mayor JR and Ni J. A static model of chip formation in microscale milling. *J Manuf Sci Eng* 2004; 126: 710–718.

Appendix

Notation

a_p	axial depth of cut
A	amplitude of vibration
d_c	critical undeformed chip thickness
d_s	tool diameter
h_{max}	maximum undeformed chip thickness
l	total grain trajectory length
l_k	cutting path length for conventional grinding
L	space between two consecutive grains

n_s	rotation rate of spindle	λ	cycle time for force repetition
s	distance between two consecutive cuts	ω_s	angular frequency of spindle
t_c	workpiece–grain contact time	ω_v	angular frequency of vibration
T	cycle duration of vibration	Φ	inclination angle
v_s	circumferential speed of tool	v_{f_x}	tool feed rate in x direction
v_w	workpiece velocity	θ	angle of grain–workpiece interaction
δ	indentation depth of a grain		